






Article

Classification of Glaucoma Based on Elephant-Herding Optimization Algorithm and Deep Belief Network

Mona A. S. Ali ^{1,2,*} , Kishore Balasubramanian ³, Gayathri Devi Krishnamoorthy ⁴ , Suresh Muthusamy ⁵,
Santhiya Pandiyan ⁶, Hitesh Panchal ⁷ , Suman Mann ⁸, Kokilavani Thangaraj ⁹, Noha E. El-Attar ¹⁰,
Laith Abualigah ^{11,*}  and Diaa Salama Abd Elminaam ^{12,13,*} 

- ¹ Computer Science Department, College of Computer Science and Information Technology, King Faisal University, Al Ahsa 400, Saudi Arabia
 - ² Computer Science Department, Faculty of Computers and Artificial Intelligence, Benha University, Benha 12311, Egypt
 - ³ Department of Electrical and Electronics Engineering, Mahalingam College of Engineering and Technology (Autonomous), Coimbatore 642001, India; bkishore1979@gmail.com
 - ⁴ Department of Electronics and Communication Engineering, NGP Institute of Technology, Coimbatore 641001, India; gayathridevi@drngpit.ac.in
 - ⁵ Department of Electronics and Communication Engineering, Kongu Engineering College (Autonomous), Coimbatore 638001, India; infostosuresh@gmail.com
 - ⁶ Department of Computer Science and Engineering, Kongu Engineering College (Autonomous), Coimbatore 638001, India; santhiyaashok172@gmail.com
 - ⁷ Department of Mechanical Engineering, Government Engineering College, Patan 384265, India; engineerhitesh2000@gmail.com
 - ⁸ Department of Information Technology, Maharaja Surajmal Institute of Technology, New Delhi 110005, India; sumanmann@msit.in
 - ⁹ Department of Electrical and Electronics Engineering, College of Engineering and Technology (Autonomous), Coimbatore 641001, India; kokime.t@gmail.com
 - ¹⁰ Department of Information System, Faculty of Computers and Artificial Intelligence, Benha University, Benha 12311, Egypt; noha.ezzat@fci.bu.edu.eg
 - ¹¹ Faculty of Computer Sciences and Informatics, Amman Arab University, Amman 11953, Jordan
 - ¹² Information Systems Department, Faculty of Computers and Artificial Intelligence, Benha University, Benha 12311, Egypt
 - ¹³ Computer Science Department, Faculty of Computer Science, Misr International University, Cairo 12585, Egypt
- * Correspondence: m.ali@kfu.edu.sa (M.A.S.A.); aligah.2020@gmail.com (L.A.); diaa.salama@mieu.egypt.edu.eg (D.S.A.E.)



Citation: Ali, M.A.S.; Balasubramanian, K.; Krishnamoorthy, G.D.; Muthusamy, S.; Pandiyan, S.; Panchal, H.; Mann, S.; Thangaraj, K.; El-Attar, N.E.; Abualigah, L.; et al. Classification of Glaucoma Based on Elephant-Herding Optimization Algorithm and Deep Belief Network. *Electronics* **2022**, *11*, 1763. <https://doi.org/10.3390/electronics11111763>

Academic Editor: Maciej Ławryńczuk

Received: 11 April 2022

Accepted: 23 May 2022

Published: 2 June 2022

Publisher's Note: MDPI stays neutral with regard to jurisdictional claims in published maps and institutional affiliations.



Copyright: © 2022 by the authors. Licensee MDPI, Basel, Switzerland. This article is an open access article distributed under the terms and conditions of the Creative Commons Attribution (CC BY) license (<https://creativecommons.org/licenses/by/4.0/>).

Abstract: This study proposes a novel glaucoma identification system from fundus images through the deep belief network (DBN) optimized by the elephant-herding optimization (EHO) algorithm. Initially, the input image undergoes the preprocessing steps of noise removal and enhancement processes, followed by optical disc (OD) and optical cup (OC) segmentation and extraction of structural, intensity, and textural features. Most discriminative features are then selected using the ReliefF algorithm and passed to the DBN for classification into glaucomatous or normal. To enhance the classification rate of the DBN, the DBN parameters are fine-tuned by the EHO algorithm. The model has experimented on public and private datasets with 7280 images, which attained a maximum classification rate of 99.4%, 100% specificity, and 99.89% sensitivity. The 10-fold cross validation reduced the misclassification and attained 98.5% accuracy. Investigations proved the efficacy of the proposed method in avoiding bias, dataset variability, and reducing false positives compared to similar works of glaucoma classification. The proposed system can be tested on diverse datasets, aiding in the improved glaucoma diagnosis.

Keywords: optic disc; optic cup; elephant-herding optimization; deep belief network; circle Hough transform; modified Wiener filter; reliefF algorithm; glaucoma

1. Introduction

Glaucoma is a type of ocular neuropathy which threatens vision if left untreated [1]. It is a gradual condition that develops as the ocular pressure rises [2]. Nearly 80 million people are affected by glaucoma globally [3]. Optic nerves are impaired gradually due to high ocular pressure [4,5]. Approximately 75–80% of the glaucoma cases are identified only at the developed stage, which cannot be cured. One cannot visualize any known symptoms of glaucoma except for narrowing of vision at a later stage [6]. The progression is slow and painful at certain levels [6]. It requires lifelong treatment, and it is impossible to reinstate vision loss. Hence, early detection of glaucoma and treatment stands as the best means of prevention. Concerning the fundamental issue, there is a critical need to build a system that can function well without the need for excessive equipment, qualified medical practitioners, or time. Computer-assisted techniques could help detect the disease at its early stages using advanced machine-learning and deep-learning methods. Trained deep-learning models could take advantage of minor changes, such as retinal layer thinning, that human specialists cannot notice.

Nevertheless, the optic nerve damage precipitated slowly develops, and as symptoms stem from it, the disease advances significantly [7]. Nevertheless, the most up-to-date technology can probably hinder glaucoma development in patients [8,9]. Figure 1 shows sample images of normal and glaucomatous eyes.



Figure 1. Eye shape (normal and glaucomatous eye).

To scrutinize various glaucoma traits, ophthalmologists utilize confocal scanning laser ophthalmoscopy (CSLO) [10], Heidelberg retina tomography (HRT), optical coherence tomography (OCT), along with fundus images [11]. For instance, numerous retinal features, optic nerves head (ONH), peripapillary atrophy, and retinal nerve fiber layer, are perceived for glaucoma diagnosis [12]. Assessment of increased IOP, abnormal visual field (V.F.), damaged ONH, etc. are usually investigated for glaucoma [13–15]. The OD is split into three disparate areas: the cup (central region), the neuroretinal rim, and parapapillary atrophy [16,17]. The white cup-like structure located in the disc center is the OC. The ratio of OC size to OD size is normally an important measure analyzed in glaucoma diagnosis, denoted as the cup-disc ratio (CDR). The main contributions of this paper can be summarized as follow:

1. Developing an optimized model employing a deep belief network classifier (DBN);
2. Employing modified Wiener filter (MWF), circular Hough transform (CHT), and Otsu's thresholding for OD and OC segmentation, respectively;
3. Generating a distinct hybrid feature set to aid in diagnosis;
4. Selecting relevant features through the ReliefF algorithm based on predictive importance weights;
5. Fine-tuning DBN by elephant-herding optimization algorithm (EHO);
6. Investigating the model's robustness to noise such as Gaussian and salt-pepper;
7. Analyzing the isolated and combined feature set contribution in glaucoma identification.

The paper is structured as follows: Section 2 outlines various works related to the proposed method. Section 3 presents the adopted architecture of the method proposed. Experimental outcomes along with dataset preparation are explored in Section 4. The conclusion is elucidated in Section 5.

2. Related Works

A brief literature review based on feature extraction and neural network classifier for glaucoma detection is elucidated in this section. Raja et al. [18] described a statistical feature extraction method based on the hyper analytic wavelet transformation (HWT) in which statistical characteristics were extracted and passed to a support vector machine (SVM). The particle swarm algorithm is used to adjust the HWT and SVM-RB simultaneously to get the optimum fit. Issac, A. et al. [19] and Koh J.E. et al. [20] presented a similar feature extraction strategy for glaucoma classification. Haralick's features-centered categorization of glaucoma using back propagation neural networks (BPNN) was suggested by Samanta et al. [21]. The results of the experiment revealed good accuracy, sensitivity, and specificity.

Acharya, U. et al. [22] proposed an effective technique that included preprocessing, picture convolving with filter banks, and the chosen features fed into the KNN classifier. Jun et al. [23] demonstrated a super-pixel-based OD and OC segmentation model for diagnosing glaucoma. The unreliable results exhibited scope for improvement. Gift and Nirmal [24] suggested gray wolf optimized NN produce enhanced accuracy for glaucoma detection through a sequence of steps. Preprocessing, image normalization and feature extraction were done, and the features were given to the GWO-NN classifier. Anushikha et al. [25] presented an automated diagnostic system utilizing wavelet features from the segmented OD, which was extorted for analysis in addition to classification. Experimental outcomes signified an accuracy of 0.947. Ajesh et al. [26] reported a new multi-feature extraction approach for glaucoma identification and classification by integrating discrete wavelet transform (DWT) and ML algorithms that produced an accuracy of 95% in glaucoma identification.

For fine-imaging analysis, DWT was computationally intensive. Diaz-Pinto et al. [27] provided an automatic technique using retinal structural features and Luv color space for OD and OC segmentation, obtaining 81% specificity and 87% sensitivity. Studies have reported numerous methodologies for recognizing glaucoma through CAD. They use either conventional machine learning, deep learning, or both. Several works related to the diagnosis of glaucoma using CNN have been demonstrated in the literature [28–32]. The CNN employed was constructed from scratch, and different datasets were used to investigate the models. Data augmentation via rotation, random flip, image translation, etc. was performed to increase the dataset size artificially. OCT images were also used to segment the retinal vasculature apart from the fundus images. The deep networks were employed to extract and learn the layer properties of the retina using a pretrained backbone network and reinforcement learning. A multiscale feature generated could then be used on modules, such as the encoder–decoder, to retrieve retinal information and capture finer retinal boundaries. Many optimization algorithms are also used to solve the various optimization problems. A blended approach is adopted in our method, where the features extracted are selected and passed to an optimized deep network for classification.

3. Proposed Method

This paper reports using the DBN classifier, a robust, novel, and efficient glaucoma detection method on retinal fundus images (RFI). Input is acquired from fundus databases and preprocessed for noise removal using MWF. Utilizing CHT, the OD is then segmented from the noise-removed image. The OC is cropped from the OD image using Otsu's thresholding algorithm. Structural and functional features are extorted and fed to the DBN classifier. The EHO algorithm optimizes DBN's parameters to obtain a minimum cost function and the best solution for healthy and glaucomatous classification. Figure 2 illustrates the schematic diagram of the system.

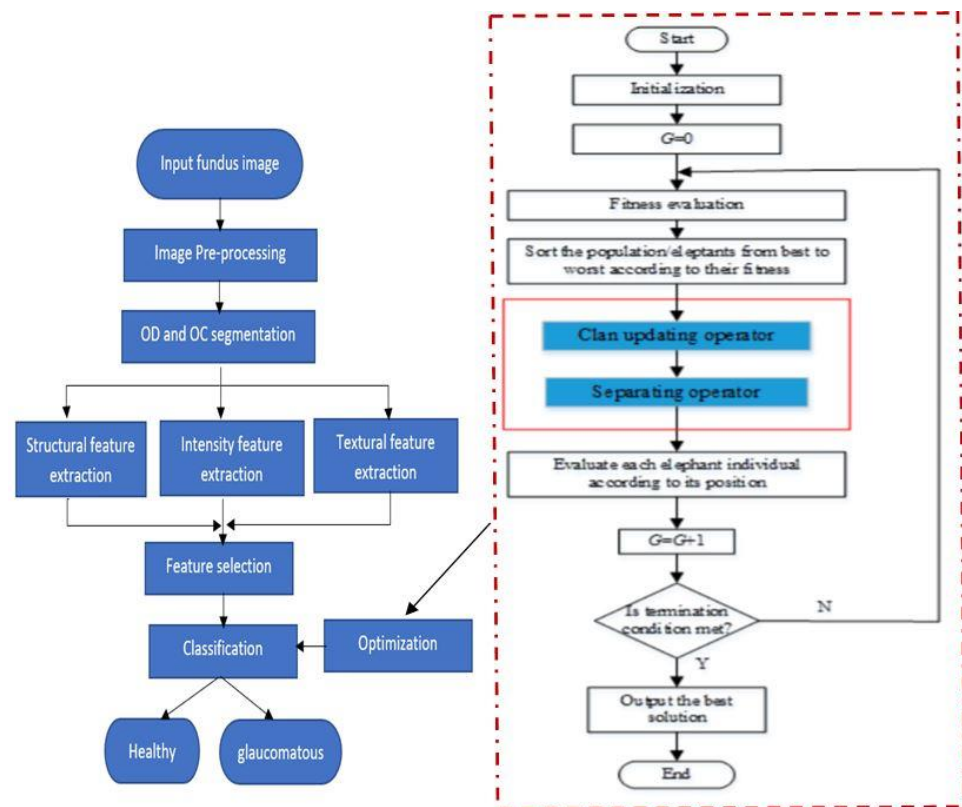


Figure 2. Flow diagram of the proposed approach.

3.1. Preprocessing

The fundus image collected must be preprocessed to highlight the vessel and other morphological features. Given the benefits of grayscale images, RGB is converted to grayscale first [33], then filtered to remove background noise [34]. A modified Wiener filter is employed to prevent impulse noise while preserving the edges [35]. The noise reduction aims to protect crucial structural content for disease detection, besides determining noisy pixels [36].

3.2. OD and OC Segmentation

OD segmentation is done on the image after noise removal. First, the OD location is identified. Subsequently, edges are calculated through the Canny edge filter. As the OD in the retina is a circular object, the circle detection Hough transform (CHT) is applied to identify the area. The boundary positions along with the region of the OD are obtained. The ROI termed OD is cropped from the original image for further OC segmentation. The OC is segmented from pre-segmented OD using Otsu’s thresholding [37].

3.3. Feature Extraction

Structural, textural, and intensity-based features contributing to the disease diagnosis are extorted in this phase [38]. Table 1 lists the set of features generated through this process.

Table 1. List of features extracted.

Structural Features	Cup to Disc Ratio (CDR), Neuro Retinal Rim (NRR), Cup Shape
Textural features	Wavelet-based features, gray level co-occurrence matrix (GLCM) features—energy, correlation, homogeneity, contrast, and entropy gray-level run length—low gray level run emphasis, gray level non-uniformity, segmentation-based fractal texture analysis (SFTA)
Intensity features	Brightness, color moments, super pixels, enhanced local binary pattern (ELBP), speeded-up robust feature (SURF), pyramid histogram of oriented gradients (PHOG), local energy-based shape histogram (LESH)

Using the procedure described above, the 111 features extracted are then selected using the relief F algorithm before being fed to DBN for classification.

3.4. Feature Selection

This stage is critical because rarely discernible characteristics are deleted, putting the modeling process under more computational strain. In this work, the ReliefF algorithm is preferred for dimensionality reduction due to its promising results, as explained in [38]. ReliefF ranks features according to their weight participation, with the most active features being placed first. As illustrated in Figure 3, other features contribute far less to the last features. As a result, we can choose the 15 most potent features based on their weight and exclude characteristics that add to the model’s computational cost.

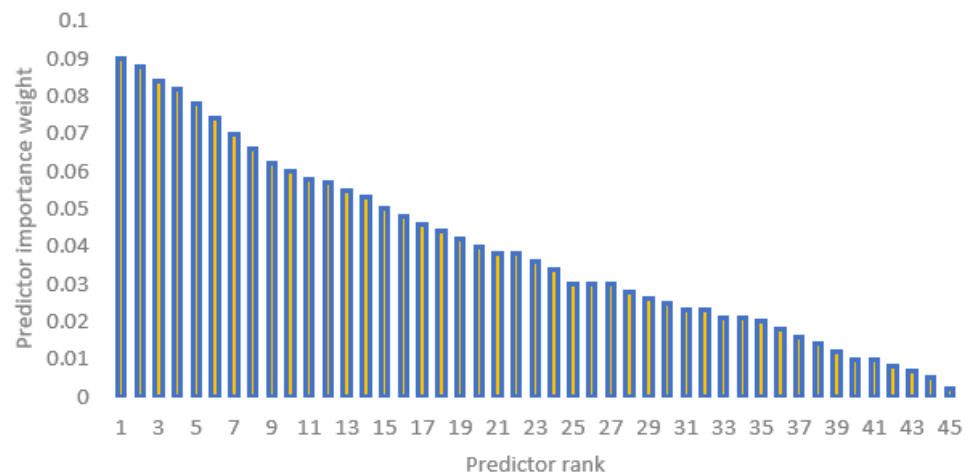


Figure 3. Weight ranking of features.

ReliefF chooses T, some instances at random, but subsequently, k searches for the closest same-class neighbors, which are referred to as the nearest hit values of H. The k-nearest neighbors are the one–one scores among the multiple classes, also known as the M(T) nearest misses. The number of nearest neighbors is set at three in our study. The 111 features are reduced to 15 optimal features based on their participation at the top of the weighted list for the highest accuracy using the procedure described above. The remaining ones are ignored because there is not much difference in output, which increases the computing weight of a model. Figure 4 depicts cumulative accuracy vs. a number of features, and 15 contribute more than the total variations.

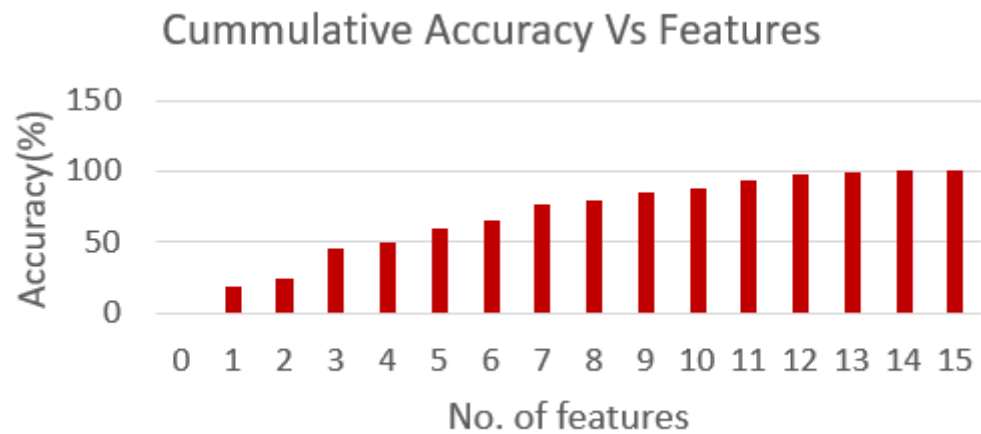


Figure 4. Cummulative accuracy vs. no. of features.

3.5. Classification

3.5.1. Deep Belief Networks (DBN)

The DBN class of neural network (NN) can be considered a generative model that uses a set of Boltzmann machines as basic building elements [39]. Each layer of the DBNs has a restricted Boltzmann machine (RBM). DBN extracts H.L. features from the data slated for training to improve the between-classes separation power. The training is performed on all the layers through supervised mode, and the backward propagation mode modifies the weight in the network to reduce over-fitting. This work develops a DBN model trained using greedy layer-wise learning [40] by stacking up RBMs, as shown in Figure 5.

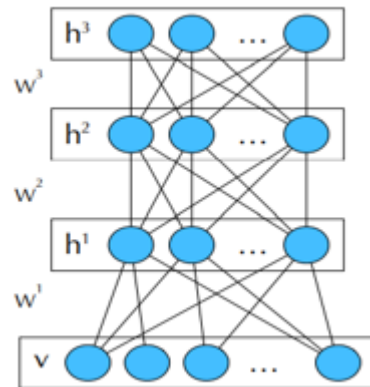


Figure 5. Stacked up RBMs model DBN.

RBM concentrates on a particular layer during its learning procedure and ignores others. We assume we have a DBN with L levels, with W_i being the RBM’s weight matrix at layer i . In addition, the hidden units at the i th layer form the layer $(i + 1)$ input unit. In the model proposed, the set of weight matrices is assigned as $W = \{W_1, W_2, W_3\}$ and the set of hidden layers as $h = \{h_1, h_2, h_3\}$. The weight matrix between layers i th and $(i + 1)$, which is denoted by W_i , while the j th hidden layer is denoted by h_j . The following energy function was used to compute the combined distribution of the hidden and visible layers:

$$p(v, h) = \frac{e^{-E(v, h)}}{\sum_{v, h} e^{-E(v, h)}} \tag{1}$$

where $E(v, h)$ denotes RBM’s energy function,

$$E(v, h) = - \sum_{i=1} a_i v_i - \sum_{j=1} b_j h_j - \sum_{i, j} v_i h_j W_{ij} \tag{2}$$

W_{ij} denotes the weight between the visible and the hidden layer, a_i and b_j describe the visible and hidden layer coefficients. This study uses the stochastic gradient descent (SGD) method following log-likelihood (L.L.) to accomplish optimal training. This is accomplished by optimizing the RBM’s parameters a , b , and w_{ij} . The derivatives of the $\log p(v, h)$ w.r.t W_{ij} , a_i and b_j must be computed to update the weights and biases. The resulting equations are

$$W^{t+1} = W^t + \eta \left(p(h | v) v^T - p(h | v) v^T \right) - \lambda W^t + \alpha \Delta W^{t-1} \tag{3}$$

$$a^{t+1} = a^t + \eta (v - \tilde{v}) + \alpha \Delta a^{t-1} \tag{4}$$

$$b^{t+1} = b^t + \eta \left(p(h | v) - p(\tilde{h} | \tilde{v}) \right) + \alpha \Delta b^{t-1} \tag{5}$$

where $p(h_j = 1 | v) = \sigma(\sum_{i=1}^m w_{ij} v_i + b_j)$, $p(v_i = 1 | h) = \sigma(\sum_{j=1}^n w_{ij} h_j + a_i)$, and $\sigma(\cdot)$ represents the logistic sigmoid function. \tilde{v} and \tilde{h} denote the reconstructed v and h , respectively.

N is the number of hidden nodes, η , the learning ratio, α , the momentum weight, and λ , the weight decay. The weight matrix and accompanying bias vectors of the visible and hidden nodes are learned using contrastive divergence (CD) and persistent contrastive divergence (PCD). This optimization process uses the BP with the conventional gradient ascent algorithm to tune the weight matrices to optimal values. The optimization algorithm considers the outcome of an extra layer built over the DBN after its previous greedy training to minimize some error metrics. Softmax, or logistic units, are frequently used in this layer.

3.5.2. Elephant Herd Optimization (EHO) Algorithm

The EHO algorithm was introduced by Wang et al. in 2015 [41]. Elephants behave socially and encompass a complex structure of calves and females. An elephant group comprises numerous clans with a matriarch as the leader and her calves or other related females. A female forms a clan. EHO concerns the succeeding assumptions.

- The elephant group is classified into clans, and each such clan comprises specific elephants.
- A specific number of male elephants (ME) depart their clan to live independently.
- Each clan has a leader termed the matriarch.

The matriarch group keeps the best solution in the elephant herd. The entire elephant population is divided into j clans. Matriarch c_i influences the new position of each elephant c_i . The elephant j in clan c_i can be calculated using

$$x_{new, c_i, j} = x_{c_{ij}} + a \times (x_{best, c_i} - x_{c_{ij}}) \times r \quad (6)$$

where $x_{new, c_i, j}$ indicated the new position and $x_{c_{ij}}$ denotes the old position for elephant j in the clan c_i . x_{best, c_i} represents matriarch c_i , which denotes the best elephant. $a \in [0,1]$ shows a scaling factor, $r \in [0,1]$. The best elephant is computed for each clan using

$$x_{new, c_i, j} = \beta \times x_{center, c_i, d} \quad (7)$$

Here, $\beta \in [0,1]$ indicates the second parameter that guides the impact of the $x_{center, c_i, d}$ delineated in

$$x_{center, c_i, d} = \frac{1}{n_{c_i}} \times \sum_{j=1}^{n_{c_i}} x_{c_i, j, d} \quad (8)$$

where $1 \leq d \leq D$, and n_{c_i} represent the number of elephants in clan c_i , $x_{c_i, j, d}$ is the d th dimension of individual elephant $x_{c_i, j, d}$ the center of clan c_i ($x_{center, c_i, d}$) can be updated (Equation (8)). The separating process could be modelled as a separation operator when tackling optimization issues. In each clan, the worst valued elephants are moved to the next position indicated by

$$x_{worst, d} = x_{min} + (x_{max} - x_{min} + 1) \times rand \quad (9)$$

Here the lower and upper bands of the search space are indicated by x_{min} and x_{max} , respectively. $rand \in [0,1]$ signifies the random value picked from the uniform distribution.

The EHO algorithm was examined for various benchmark set functions and in medical diagnosis [42–46], showing better results. This study employs the EHO algorithm for DBN parameter optimization. The output of the DBN model is grounded in weights and the biases of preceding layers in the network. EHO does not employ the previous individuals in the later updating process as other optimization algorithms. EHO is a swarm-inspired algorithm that deals with global optimization missions characterized by clan updating and searching operations. EHO does not resort to relaxation and is less vulnerable to noise. They perform better in constrained, optimized environments. High convergence rate and low localization errors with less execution time are the important characteristics of EHO. The algorithm can tackle non-convex ML problems directly.

3.5.3. Fine Tuning of DBM

The learning rate, hidden units, momentum weight, and weight decay are the four basic parameters set up in most RBMs. The use of traditional methods for computing the error function is an NP-hard problem due to its complexity and differentiation. Meta-heuristics have been employed to solve this issue. The EHO algorithm is used to optimize the DBN training by fine tuning the parameters in this work. Here, the parameters set are

$$n \in [5, 100], \eta \in [0.1, 0.9], \lambda \in [0.1, 0.9] \text{ and } \alpha \in [0.00001, 0.01]$$

A fitness function must be designed to steer the searching process to attain the best answers to meet the objectives. Mean squared error (*MSE*) is adopted as the fitness function. It measures the error between the output and the desired value and is given by

$$MSE = \frac{1}{T} \sum_{j=1}^N \sum_{i=1}^T (D_j(i) - Y_j(i))^2 \quad (10)$$

where T —data number, N —number of the output layers.

The EHO looks for a collection of DBN parameters that minimizes *MSE*. $D_j(i)$ denotes the value from the j th unit in the DBN's output layer at the time 't', $Y_j(i)$ represents the j th factor of the desired value. The process is repeated until the halting criteria is met.

The optimization steps of EHO are as follows:

1. Set the EHO parameters and initialize the population.
2. Evaluate the individual fitness value (RMSE) of the DBN, as per the learning rate and the number of batch learning. Identify the optimal individual.
3. Check if the termination condition is reached; if so, end the iteration and output the result; or else, go to the next step.
4. Update each individual position. Reinitialize the individuals beyond the lower and upper limits.
5. Start a new iteration by updating the optimal individual.

4. Results and Discussion

Evaluation of the proposed model's performance is presented in this section. The experiment is executed in MATLAB with the following specifications: the Intel Core i7 Processor, Windows 10, 3.20 GHz CPU speed, and 4GB RAM.

4.1. Dataset Preparation

This work uses DRISHTI-GS1, ACRIMA, ORIGA-Light, and LAG datasets for evaluation. The images were captured utilizing a Canon CR-1 fundus camera at 2336×3504 resolution with a 45° FOV and a disparate acquisition setting. The dataset used in the methodology is from public and private datasets annotated by an ophthalmologist who has over 15 years of experience in the field. The list of databases is depicted in Table 2. A total of 7280 images obtained from various public and private databases are used for investigating the proposed system's performance after eliminating a few irrelevant images. Images are trained and tested in the ratio of 70:30, respectively.

Table 2. Dataset labeling.

Database/Images	Normal	Glaucoma	Total	Type
DRISHIT-GSI [44]	12	89	101	Public
ACRIMA [29,45]	309	396	705	Public
OTIHS-lihgy [46]	482	368	650	Public
LAG [47]	3432	2392	5824	Private
Total	4235	3045	7280	

Images that are preprocessed are subjected to OD and OC segmentation. Sample images and results of the segmentation are given below in Figure 6.

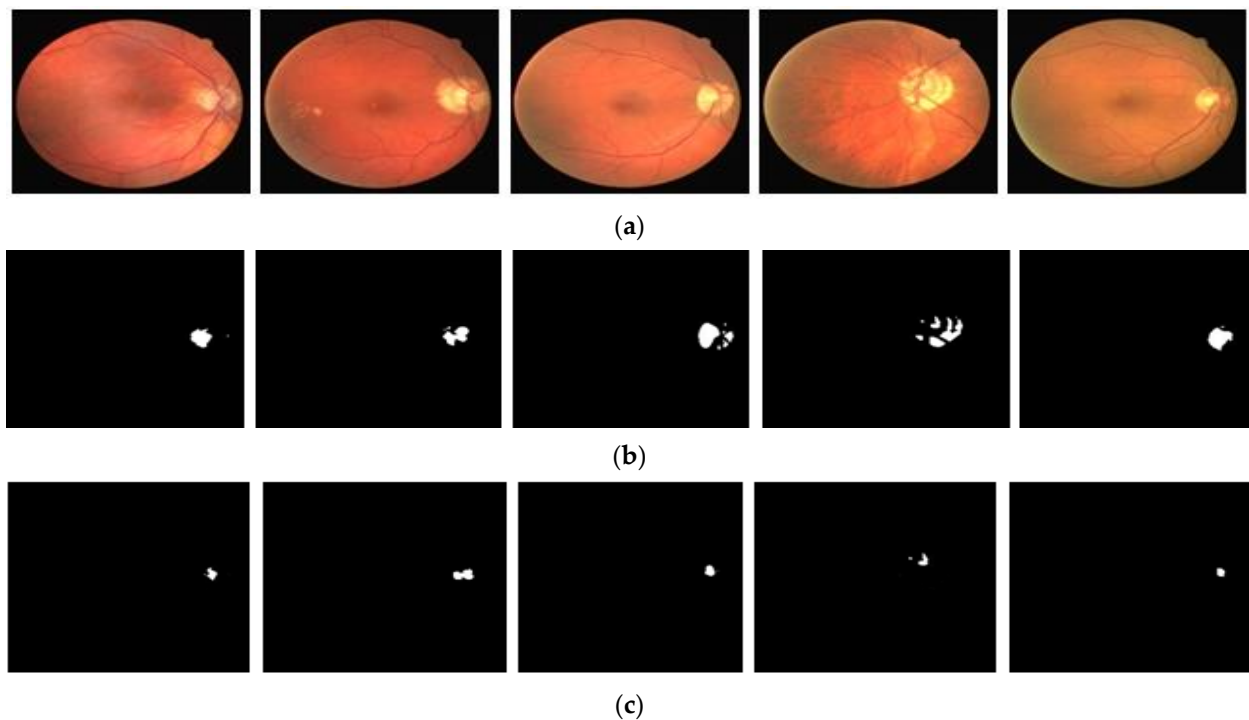


Figure 6. Results: (a) original image; (b) OD segmented image; (c) OC segmented image.

4.2. Performance Analysis

Experiments are done to show the efficacy of the DBN–EHO on different fundus datasets. Initially, the investigations are performed to show the efficacy of EHO in optimizing the DBN. EHO is compared with meta-heuristic algorithms, such as artificial bee colony (ABC), firefly algorithm (FA), harmony search (HS), cuckoo search (CS), particle swarm optimization algorithms (PSO), and differential evolution algorithms (DE). A hold-out technique with 20 training and test sets generated at random, subjected to 10 iterations for each RBM learning procedure, and a mini-batch of 20 are performed for consistent comparisons with other works. Five agents of over 50 iterations are employed to achieve convergence using all strategies in tests. Control parameters for all the algorithms are outlined in Table 3.

Table 3. Control parameters of all algorithms.

Algorithm	Parameters
ABC	$N = 30, MCN = 100, \text{limit} = 20$
HS	$HMCR = 0.7, PAR = 0.7, \eta = 1$
FA	$\gamma = 1, \beta_0 = 1, \alpha = 0.2, MCN = 100$
CS	$\alpha = 0.1, pa = 0.25$
PSO	$W_{\max} = 0.9, W_{\min} = 0.2, C1 = 2, C2 = 2$
DE	$F = 0.8, C = 0.5$
EHO	$nClan = 5, \alpha = 0.25, \beta = 0.05$

In Table 4, the MSE values of each algorithm on the original LAG dataset considering DBN. A Wilcoxon signed-rank test with a 0.05 significance level is utilized to analyze the method statistically. It is observed from Table 4 that EHO outperformed all the other

algorithms in terms of the lowest MSE employing fewer layers. ABC and FA algorithms have also performed well next to EHO.

Table 4. Average MSE over the LAG dataset.

Algorithm	Layer-1		Layer-2		Layer-3	
	CD	PCD	CD	PCD	CD	PCD
ABC	0.0891	0.8940	0.0881	0.0884	0.0880	0.0878
HS	0.1259	0.1345	0.1256	0.1169	0.1158	0.1156
FA	0.0864	0.0864	0.864	0.0860	0.0864	0.0862
CS	0.1146	0.1146	0.1176	0.1175	0.1164	0.1162
PSO	0.1086	0.1086	0.0988	0.0992	0.1045	0.1046
DE	0.1250	0.1254	0.1254	0.1254	0.1158	0.1156
EHO	0.0756	0.0756	0.0778	0.0778	0.0776	0.774

Taking the performance of EHO, the performance of the proposed work is assessed by finding ‘true positive’ (*TP*), ‘true negative’ (*TN*), ‘false positive’ (*FP*), and ‘false negative’ (*FN*) values. *TP* denotes the instances wherein glaucoma is detected correctly. *TN* shows the condition wherein a person with no glaucoma is classified correctly. *FP* indicates the number of negative instances recognized as positive. Positive instances recognized as negative are indicated by *FN*. Precision, accuracy, F-score, specificity, recall, sensitivity, and MCC (Mathew’s correlation coefficient) are used in this work, as in Table 5.

Table 5. Performance Metrics.

Parameters	Expression
Sensitivity (%)	$\frac{TP}{TP+FN} \times 100$
Specificity (%)	$\frac{TN}{TN+FP} \times 100$
Accuracy (%)	$\frac{TP+TN}{TP+FN+TN+FP} \times 100$
Precision (%)	$\frac{TP}{TP+FP} \times 100$
Recall (%)	$\frac{TP}{TP+FN} \times 100$
F-score (%)	$2 \times \frac{(Precision)(Recall)}{Precision+Recall} \times 100$
Mathew’s correlation coefficient (MCC) (%)	$\frac{(TP \times TN) - (FP \times FN)}{\sqrt{(TP+FP)(TP+FN)(TN+FP)(TN+FN)}} \times 100$

The performance of the proposed work on individual datasets is provided in Table 6. It is inferred that a maximum accuracy of 99.34% on the ACRIMA dataset is attained, followed by 99.31% on the LAG dataset. The classification rate is between 96.95% and 99.34%, ensuring that the DBN–EHO performed better in all the datasets. This indicates that the images in the set are captured under different illuminations. Specificity of 100% on the LAG dataset shows that the model can reduce false positive rates.

Table 6. Performance of the proposed method employing DBN and EHO.

Dataset	Acc (%)	Sens (%)	Spec (%)	Prec (%)	Recall (%)	F-Score (%)	MCC
Drishti-GS1	96.95	98.56	97.44	97.69	96.86	97.68	0.749
ACRIMA	99.34	97.1	98.2	88.92	95.3	93.5	0.772
ORIGA	98.51	94.73	98.7	98.55	97.92	95.32	0.784
LAG	99.31	99.89	100	96.73	94.56	95.64	0.789

The impact of isolated and combined feature sets on the diagnosis of glaucoma in the LAG dataset is depicted in Table 7. The extraction of isolated features yielded an enhanced result, increasing the algorithm’s efficiency. When the features are combined, an accuracy of 99.3% is obtained. When the features are combined, better accuracy of 99.34% is obtained. The feature contribution indicates that the DBN optimization also contributes to appreciable performance as the accuracy ranges from 95% to 99% on different kinds of features.

Table 7. Impact of features in detecting glaucoma from LAG dataset.

Features	Accuracy (%)	Sensitivity (%)	Specificity (%)
Structural (SF)	94.87	95.32	93.52
Intensity (IF)	95.98	89.23	92.41
Textural (TF)	96.21	97.28	99.33
SF + IF	95.86	90.74	95.21
SF + TF	96.78	94.23	97.56
IF + TF	90.88	95.79	94.35
Selected features	99.31	99.89	100

The feature contribution indicates that the DBN optimization also contributes to appreciable performance as the accuracy ranges from 95% to 99% on different kinds of features. A 10-fold cross validation done to reduce bias during testing enhances the algorithm’s robustness and reduces the classifier’s misclassification rate. From Table 8, it is seen that the cross-validation accuracy across the datasets is appreciably high, ensuring that the model is free from bias. The model applies to a wide range of datasets, compensating for any imbalance. Figure 7 highlights the proposed work against various performance metrics.

Table 8. 10-fold cross validation results.

Dataset	Accuracy (%)
Drishti-GS1	97.1
ACRIMA	98.5
ORIGA	96.2
LAG	97.8

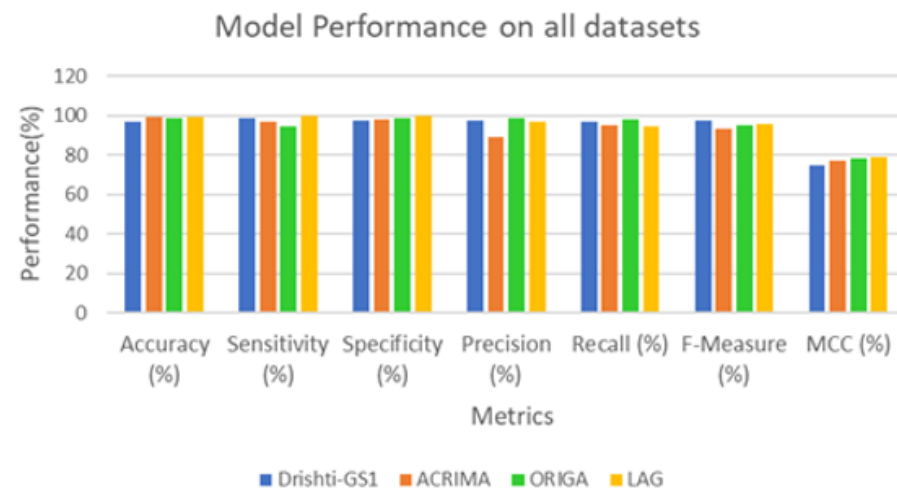


Figure 7. Results of the proposed work on all the datasets.

A 10-fold CV is carried out to reduce bias during testing, and the results are shown in Table 8.

From Table 8, it is seen that the cross-validation accuracy across the datasets is appreciably high, ensuring that the model is free from bias. The model applies to a wide range of datasets, compensating for any imbalance.

Table 9 reports the outcomes of the classifier when compared with similar conventional ML classifiers, such as K-nearest neighbor (KNN), random forest (RF), support vector machine (SVM), and DBN without optimization. The DBN attains a more appreciable performance than the conventional ML classifiers. The DBN, when optimized for weight by EHO, still achieves better performance across all the datasets.

Table 9. Performance analysis with dissimilar classifiers.

Dataset	Classifier	Accuracy (%)	Sensitivity (%)	Specificity (%)
Drishti-GS	KNN	95.34	90.47	93.08
	RF	94.50	91.34	92.33
	SVM	95.86	96.87	96.87
	DBN	96.23	97.56	96.62
	DBN-EHO	96.95	98.56	97.44
ACRIMA	KNN	95.66	90.86	93.78
	RF	94.32	91.24	90.84
	SVM	97.06	96.64	96.12
	DBN	97.26	98.16	97.06
	DBN-EHO	99.34	97.1	98.2
ORIGA-Light	KNN	94.22	96.86	97.08
	RF	91.34	88.56	89.75
	SVM	94.88	95.56	96.69
	DBN	96.06	97.65	97.81
	DBN-EHO	98.51	94.73	98.7
LAG	KNN	94.24	95.56	95.85
	RF	92.78	90.89	91.48
	SVM	95.60	95.68	96.45
	DBN	97.54	95.67	97.43
	DBN-EHO	99.31	100	99.89

From Table 9, it is seen that the DBN classifier attains a more appreciable performance than the conventional ML classifiers. The DBN, when optimized for weight by EHO, still achieves better performance across all the datasets. Furthermore, to assess the robustness of the model, salt-pepper and Gaussian noise are added to the LAG dataset (original image set). Gaussian noise is predominant if the images were captured under low illumination. Salt-pepper noise is an impulse noise occurring owing to intense and sparse disturbances. Figure 8 depicts the original and noise-added image (sample). Experimentation is performed with Gaussian noise and salt-pepper noise, with the variance (σ) and noise density (d) varying from 0.1 to 0.5, respectively, and the result is reported in Figure 9.

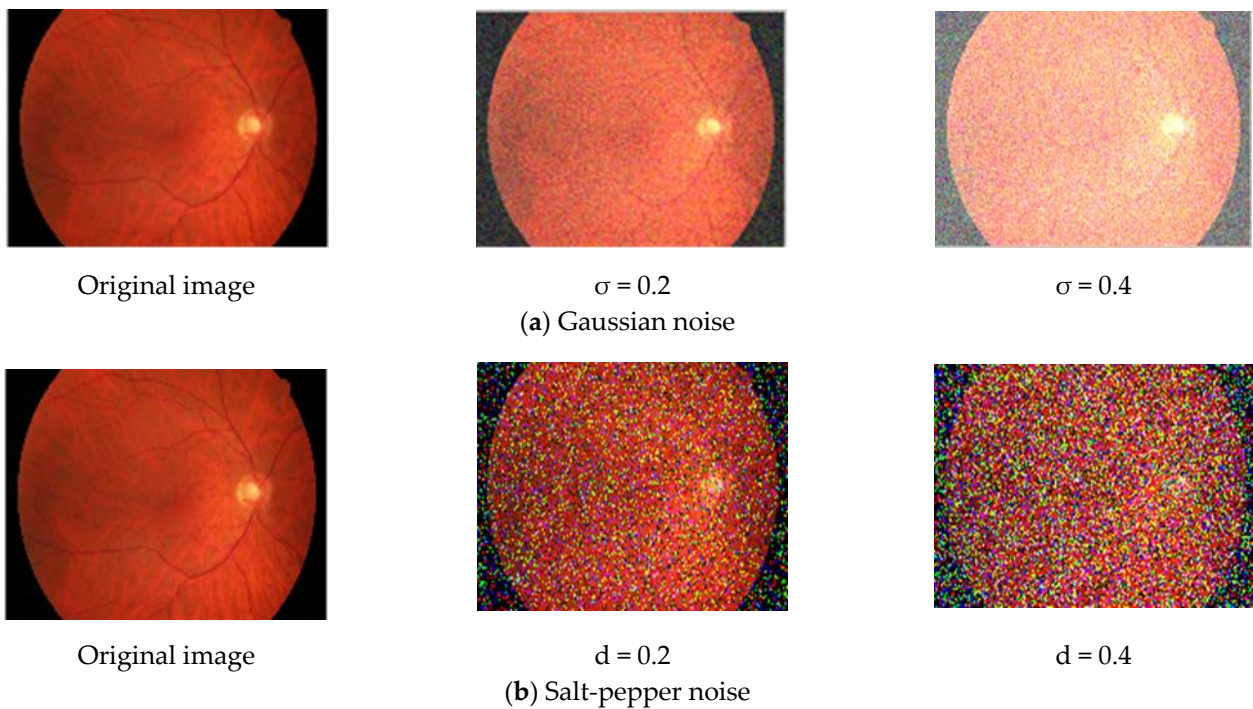


Figure 8. Sample fundus images with noise added.

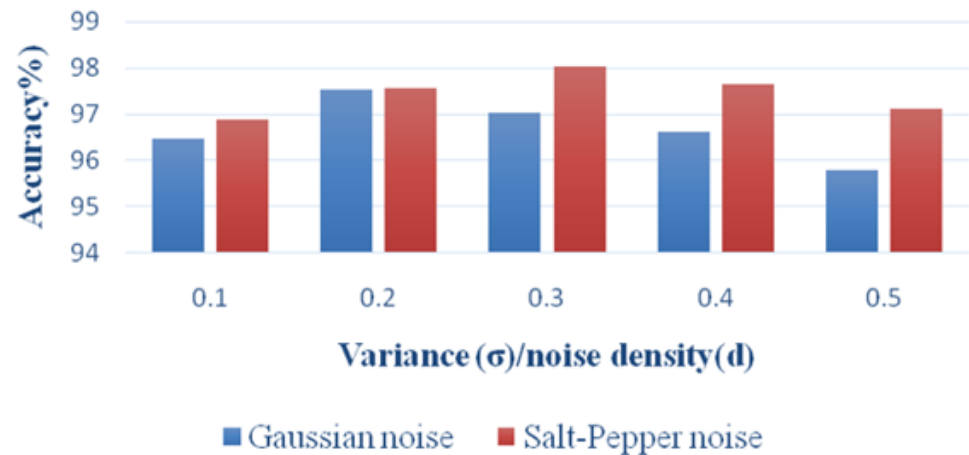


Figure 9. Recognition rate on degraded images of the LAG dataset.

It is seen from Figure 9 that the accuracy remains fairly the same. This demonstrates that the suggested model is extremely robust in both original and degraded datasets.

Table 10 compares the proposed model with well-known CNN models employing transfer learning. Transfer learning is applied to the DRISHTI-GS1 dataset, as the number of images is small. It is inferred that our model can work well compared to well-known, pre-trained models using transfer learning. Table 11 illustrates a comparison of similar other techniques and our technique in diagnosing glaucoma. Many optimization algorithms are also used to solve the other various optimization problems [48–64].

Table 10. Comparison of DBN-EHO with CNN models employing transfer learning.

Dataset	Classifier	Accuracy (%)	Sensitivity (%)	Specificity (%)
Drishti-GS	AlexNet	93.84	91.57	92.88
	GoogLeNet	95.46	90.34	93.36
	VGG16	94.12	95.77	96.42
	DBN-EHO	96.95	98.56	97.44

Table 11. Comparison of proposed work.

References	Features/Methods	Classifier Used	Images	Performance (%)
Karthikeyan and Rengarajan [65]	GLCM	BPN	Local dataset	Accuracy—95
Issac, A. et al. [19]	CDR, NRR, blood vessel features	SVM and ANN	67	Accuracy—94.11 Sensitivity—100
Mookiah et al. [66]	Discrete wavelet and HOS	SVM	60	Accuracy—95 Sensitivity—93.3 Specificity—96.67
Gifta [24]	GLCM, HOG, SURF	Gray Wolf Optimized NN	N.A.	Accuracy—93.1 Sensitivity—91.6 Specificity—94.1
Acharya, U.R. et al. [22]	6 features from LM filter bank	KNN	NA	Accuracy—95.8
Koh, J.E. et al. [20]	PHOG, SURF features	KNN	910	Accuracy—96.21 Sensitivity—97.42
Samanta et al. [21]	Haralick features	BPN	60	Accuracy—96.26 Sensitivity—90.43 Specificity—99.5
Acharya et al. [67]	Texture and HOF	RF	60	Accuracy—91
Acharya et al. [68]	Gabor transformation and principal component analysis	SVM	510	Accuracy—93.10; sensitivity—89.75; specificity—96.20
Yadav et al. [69]	Homogeneity, Contrast, energy, correlation, entropy	N.N.	20	Accuracy—72
Maheshwari et al. [70]	Entropy and fractal	SVM	488	Accuracy—95.19
Bajwa M. N et al. [71]	ROI, Scaling	2-Stage CNN	ORIGA	AUC—0.87
Raghavendra et al. [72]	-	20 layer CNN	1426	Accuracy—98.13
Chen et al. [73]	-	16 layer CNN	SECS, ORIGA	AUC—0.881
Proposed Work	Structural, intensity, and texture features	DBN and EHO	7280	Accuracy—99.34 Sensitivity—100 Specificity—99.89

5. Conclusions

Glaucoma is a class of ocular neuropathy wherein the optic nerve gets vandalized, resulting in permanent vision loss. Glaucoma detection in RFI using the DBN classifier is proposed in this work. Input images from different public databases are enhanced through the preprocessing phase. The OD and OC are then segmented using CHT and Otsu's thresholding. The various structural, intensity, and textural features are extorted from the segmented OC and OD images and fed to the DBN classifier optimized by the EHO algorithm. To investigate the performance, the technique is compared with classifier techniques,

such as R.F., KNN, SVM, pre-trained CNNs, etc. Experimental outcomes exhibit the performance of the DBN classifier in recognizing the absence or presence of glaucoma accurately compared to other approaches. The proposed work concentrates on some of the important features contributing to glaucoma disease. The ReliefF algorithm selects the features before feeding them to the classifier for classifying them into either healthy or glaucomatous. The classifier performance is improved through an optimization technique where EHO does the weight update process. Dataset imbalance is also minimized as the model showed better training accuracy when images were selected randomly from each set using 10-fold cross validation. One potential drawback of this method is that it is unclear whether the attained specificities and sensitivities will be generalizable to real-world patient populations with common comorbidities, such as cataracts and surface ocular disease, which can degrade the input image quality. The performance of the computational hardware needs to be improved, along with network structure refinement and data dimension reduction, to attain competitively better computational speed. In the future, a universal domain adaptation method for various datasets (both public and private) is needed to be developed using hybrid weighted deep adversarial learning [74] and adaptive on-line validation [75]. In the future, the detection of glaucoma systems will be enhanced using the feature selection and ranking phase with different hybrid optimization algorithms. Besides, granular computing will be embedded in deep neural networks (granulated CNN) to enhance the computation speed significantly.

Author Contributions: Conceptualization, M.A.S.A., D.S.A.E., N.E.E.-A. and L.A.; methodology, M.A.S.A., D.S.A.E., N.E.E.-A. and L.A.; software, M.A.S.A., D.S.A.E., N.E.E.-A. and L.A.; validation K.B., G.D.K., S.M. (Suresh Muthusamy), S.P., H.P., S.M. (Suman Mann) and K.T.; formal analysis, K.B., G.D.K., S.M. (Suresh Muthusamy), S.P., H.P., S.M. (Suman Mann) and K.T.; investigation, M.A.S.A., D.S.A.E., N.E.E.-A. and L.A.; resources, M.A.S.A., D.S.A.E., N.E.E.-A. and L.A.; data curation, M.A.S.A., D.S.A.E., N.E.E.-A. and L.A.; writing—original draft preparation, K.B., G.D.K., S.M. (Suresh Muthusamy), S.P., H.P., S.M. (Suman Mann) and K.T.; writing—review and editing, M.A.S.A., D.S.A.E., N.E.E.-A. and L.A.; visualization, M.A.S.A., D.S.A.E., N.E.E.-A. and L.A.; project administration, D.S.A.E.; funding acquisition, M.A.S.A. All authors have read and agreed to the published version of the manuscript.

Funding: This Research is funded by Deanship of Scientific Research, King Faisal University, Saudi Arabia [Project No. GRANT716].

Acknowledgments: This work was supported by the Deanship of Scientific Research, Vice Presidency for Graduate Studies and Scientific Research, King Faisal University, Saudi Arabia [Project No. GRANT716].

Conflicts of Interest: The authors declare no potential conflicts of interest and funding.

References

1. Quigley, H.A.; Broman, A.T. The number of people with glaucoma worldwide in 2010 and 2020. *Br. J. Ophthalmol.* **2006**, *90*, 262–267. [[CrossRef](#)] [[PubMed](#)]
2. Dervisevic, E.; Pavlja, S.; Dervisevic, A.; Kasumovic, S.S. Challenges in early glaucoma detection. *Med. Arch.* **2017**, *70*, 203–207. [[CrossRef](#)] [[PubMed](#)]
3. Kassebaum, N.J.; Bertozzi-Villa, A.; Coggeshall, M.S.; A Shackelford, K.; Steiner, C.; Heuton, K.R.; Gonzalez-Medina, D.; Barber, R.; Huynh, C.; Dicker, D.; et al. Global, regional, and national levels and causes of maternal mortality during 1990–2013: A systematic analysis for the Global Burden of Disease Study 2013. *Lancet* **2014**, *384*, 980–1004. [[CrossRef](#)]
4. What Is Glaucoma? Available online: <https://www.glaucoma.org/glaucoma/optic-nerve-cupping.php> (accessed on 1 May 2021).
5. McMonnies, C.W. Intraocular pressure and glaucoma: Is physical exercise beneficial or a risk? *J. Optom.* **2016**, *9*, 139–147. [[CrossRef](#)]
6. Types of Glaucoma. Available online: <http://www.glaucoma-association.com/about-glaucoma/types-of-glaucoma/chronic-glaucoma> (accessed on 1 May 2021).
7. Blindness. Available online: <https://www.who.int/health-topics/blindness-and-vision-loss> (accessed on 2 May 2021).
8. Chandrika, S.; Nirmala, K. Analysis of CDR detection for glaucoma diagnosis. *Int. J. Eng. Res. Appl.* **2014**, *2*, 23–27.

9. Al-Bander, B.; Al-Nuaimy, W.; Al-Tae, M.; Zheng, Y. Automated glaucoma diagnosis using deep learning approach. In Proceedings of the 14th International Multi-Conference on Systems, Signals & Devices (SSD), Marrakech, Morocco, 28–31 March 2017; pp. 207–210.
10. Mardin, C.Y.; Horn, F.K.; Jonas, J.B.; Budde, W.M. Preperimetric glaucoma diagnosis by confocal scanning laser tomography of the optic disc. *Br. J. Ophthalmol.* **1999**, *83*, 299–304. [[CrossRef](#)]
11. Adhi, M.; Duker, J.S. Optical coherence tomography—Current and future applications. *Curr. Opin. Ophthalmol.* **2013**, *24*, 213–221. [[CrossRef](#)]
12. Septiarini, A.; Khairina, D.M.; Kridalaksana, A.H.; Hamdani, H. Automatic Glaucoma Detection Method Applying a Statistical Approach to Fundus Images. *Healthc. Inform. Res.* **2018**, *24*, 53–60. [[CrossRef](#)]
13. Thorat, S.; Jadhav, S. Optic disc and cup segmentation for glaucoma screening based on super pixel classification. *Int. J. Innov. Adv. Comput. Sci.* **2015**, *4*, 167–172.
14. Kavitha, K.; Malathi, M. Optic disc and optic cup segmentation for glaucoma classification. *Int. J. Adv. Res. Comput. Sci. Technol.* **2014**, *2*, 87–90. [[CrossRef](#)]
15. Manju, K.; Sabeenian, R.S. Robust CDR calculation for glaucoma identification. *Biomed. Res.* **2018**. [[CrossRef](#)]
16. Mahalakshmi, V.; Karthikeyan, S. Clustering based optic disc and optic cup segmentation for glaucoma detection. *Int. J. Innov. Res. Comput. Commun. Eng.* **2014**, *2*, 3756–3761.
17. Almazroa, A.; Burman, R.; Raahemifar, K.; Lakshminarayanan, V. Optic Disc and Optic Cup Segmentation Methodologies for Glaucoma Image Detection: A Survey. *J. Ophthalmol.* **2015**, *2015*, 180972. [[CrossRef](#)] [[PubMed](#)]
18. Raja, C.; Gangatharan, N. A Hybrid Swarm Algorithm for optimizing glaucoma diagnosis. *Comput. Biol. Med.* **2015**, *63*, 196–207. [[CrossRef](#)] [[PubMed](#)]
19. Issac, A.; Sarathi, M.P.; Dutta, M.K. An adaptive threshold based image processing technique for improved glaucoma detection and classification. *Comput. Methods Programs Biomed.* **2015**, *122*, 229–244. [[CrossRef](#)]
20. Koh, J.E.W.; Ng, E.Y.K.; Bhandary, S.V.; Laude, A.; Acharya, U.R. Automated detection of retinal health using PHOG and SURF features extracted from fundus images. *Appl. Intell.* **2017**, *48*, 1379–1393. [[CrossRef](#)]
21. Samanta, S.; Ahmed, S.K.; Salem, M.A.; Nath, S.S.; Dey, N.; Chowdhury, S.S. Haralick features based automated glaucoma classification using back propagation neural network. In Proceedings of the 3rd International Conference on Frontiers of Intelligent Computing: Theory and Applications (FICTA), Bhubaneswar, India, 14–15 November 2014; Springer: Cham, Switzerland, 2015; pp. 351–358.
22. Cheng, J.; Liu, J.; Xu, Y.; Yin, F.; Wong, D.W.; Tan, N.M.; Tao, D.; Cheng, C.Y.; Aung, T.; Wong, T.Y. Superpixel classification based optic disc and optic cup segmentation for glaucoma screening. *IEEE Trans. Med. Imaging* **2013**, *32*, 1019–1032. [[CrossRef](#)]
23. Singh, A.; Dutta, M.K.; ParthaSarathi, M.; Uher, V.; Burget, R. Image processing based automatic diagnosis of glaucoma using wavelet features of segmented optic disc from fundus image. *Comput. Methods Programs Biomed.* **2016**, *124*, 108–120. [[CrossRef](#)]
24. Ajesh, F.; Ravi, R.; Rajakumar, G. Early diagnosis of glaucoma using multi-feature analysis and DBN based classification. *J. Ambient. Intell. Humaniz. Comput.* **2021**, *12*, 4027–4036. [[CrossRef](#)]
25. Diaz, A.; Morales, S.; Naranjo, V.; Alcocer, P.; Lanzagorta, A. Glaucoma diagnosis by means of optic cup feature analysis in color fundus images. In Proceedings of the 24th European Signal Processing Conference (EUSIPCO), Budapest, Hungary, 29 August–2 September 2016; pp. 2055–2059.
26. Gómez-Valverde, J.J.; Antón, A.; Fatti, G.; Liefers, B.; Herranz, A.; Santos, A.; Sánchez, C.I.; Ledesma-Carbayo, M.J. Automatic glaucoma classification using color fundus images based on convolutional neural networks and transfer learning. *Biomed. Opt. Express* **2019**, *10*, 892–913. [[CrossRef](#)]
27. Diaz-Pinto, A.; Morales, S.; Naranjo, V.; Köhler, T.; Mossi, J.M.; Navea, A. CNNs for automatic glaucoma assessment using fundus images: An extensive validation. *Biomed. Eng. Online* **2019**, *18*, 29. [[CrossRef](#)] [[PubMed](#)]
28. Raghavendra, U.; Fujita, H.; Bhandary, S.V.; Gudigar, A.; Tan, J.H.; Acharya, U.R. Deep convolution neural network for accurate diagnosis of glaucoma using digital fundus images. *Inf. Sci.* **2018**, *441*, 41–49. [[CrossRef](#)]
29. Orlando, J.I.; Prokofyeva, E.; del Fresno, M.; Blaschko, M.B. Convolutional neural network transfer for automated glaucoma identification. In Proceedings of the 12th International Symposium on Medical Information Processing and Analysis, Tandil, Argentina, 5–7 December 2016.
30. Chen, X.; Xu, Y.; Wong, D.W.; Wong, T.Y.; Liu, J. Glaucoma detection based on deep convolutional neural network. In Proceedings of the 2015 37th annual international conference of the IEEE engineering in medicine and biology society (EMBC), Milan, Italy, 25–29 August 2015; pp. 715–718.
31. Staal, J.; Abramoff, M.D.; Niemeijer, M.; Viergever, M.A.; Van Ginneken, B. Ridge-based vessel segmentation in color images of the retina. *IEEE Trans. Med. Imaging* **2004**, *23*, 501–509. [[CrossRef](#)]
32. Hani, A.F.; Soomro, T.A.; Fayee, I.; Kamel, N.; Yahya, N. Identification of noise in the fundus images. In Proceedings of the 2013 IEEE International Conference on Control System, Computing and Engineering, Penang, Malaysia, 29 November–1 December 2013; pp. 191–196.
33. Nagu, M.; Shanker, N. Image De-Noising by Using Median Filter and Wiener Filter. *Int. J. Innov. Res. Comput. Commun. Eng.* **2014**, *2*, 5641–5649.
34. Aliskan, A.; Çevik, U. An Efficient Noisy Pixels Detection Model for C.T. Images using Extreme Learning Machines. *Teh. Vjesn.—Tech. Gaz.* **2018**, *25*, 679–686. [[CrossRef](#)]

35. Raj, P.A.; George, A. FCM and Otsu's Thresholding based Glaucoma Detection and its Analysis using Fundus Images. In Proceedings of the 2nd International Conference on Intelligent Computing, Instrumentation and Control Technologies (ICICICT), Kannur, India, 5–6 July 2019; pp. 753–757.
36. Urbanowicz, R.J.; Meeker, M.; La Cava, W.; Olson, R.S.; Moore, J.H. Relief-based feature selection: Introduction and review. *J. Biomed. Inform.* **2018**, *85*, 189–203. [[CrossRef](#)]
37. Rosa, G.; Papa, J.; Costa, K.; Passos, L.; Pereira, C.; Yang, X. Learning Parameters in Deep Belief Networks Through Firefly Algorithm. In Proceedings of the IAPR Workshop on Artificial Neural Networks in Pattern Recognition. In Artificial Neural Networks in Pattern Recognition. ANNPR 2016, Ulm, Germany, 28–30 September 2016; Lecture Notes in Computer Science. Springer: Cham, Switzerland, 2016; pp. 138–149.
38. Hinton, G.E.; Osindero, S.; Teh, Y.-W. A Fast Learning Algorithm for Deep Belief Nets. *Neural Comput.* **2006**, *18*, 1527–1554. [[CrossRef](#)]
39. Wang, G.-G.; Deb, S.; Coelho, L.d.S. Elephant Herding Optimization. In Proceedings of the 3rd International Symposium on Computational and Business Intelligence (ISCBI 2015), Bali, Indonesia, 7–8 December 2015; pp. 1–5.
40. Li, J.; Lei, H.; Alavi, A.H.; Wang, G.-G. Elephant Herding Optimization: Variants, Hybrids, and Applications. *Mathematics* **2020**, *8*, 1415. [[CrossRef](#)]
41. Nayak, M.; Das, S.; Bhanja, U.; Senapati, M.R. Elephant herding optimization technique based neural network for cancer prediction. *Inform. Med. Unlocked* **2020**, *21*, 100445. [[CrossRef](#)]
42. Sivaswamy, J.; Krishnadas, S.R.; Joshi, G.D.; Jain, M.; Tabish, A.U.S. Drishti-GS: Retinal image dataset for optic nerve head (ONH) segmentation. In Proceedings of the IEEE 11th International Symposium on Biomedical Imaging (ISBI), Beijing, China, 29 April–2 May 2014; pp. 53–56.
43. Khan, S.M.; Liu, X.; Nath, S.; Korot, E.; Faes, L.; Wagner, S.K.; Keane, P.A.; Sebire, N.J.; Burton, M.J.; Denniston, A.K. A global review of publicly available datasets for ophthalmological imaging: Barriers to access, usability, and generalisability. *Lancet. Digit. Health* **2021**, *3*, e51–e66. [[CrossRef](#)]
44. Zhang, Z.; Yin, F.S.; Liu, J.; Wong, W.K.; Tan, N.M.; Lee, B.H.; Cheng, J.; Wong, T.Y. ORIGA^(light): An on-line retinal fundus image database for glaucoma analysis and research. In Proceedings of the 2010 Annual International Conference of the IEEE Engineering in Medicine and Biology, Buenos Aires, Argentina, 31 August–4 September 2020; pp. 3065–3068.
45. Li, L.; Xu, M.; Wang, X.; Jiang, L.; Liu, H. Attention Based Glaucoma Detection: A Large-Scale Database and CNN Model. In Proceedings of the IEEE/CVF Conference on Computer Vision and Pattern Recognition (CVPR), Long Beach, CA, USA, 15–20 June 2019; pp. 10563–10572.
46. Karthikeyan, S.; Rengarajan, N. Performance Analysis of Gray Level Co-Occurrence Matrix Texture Features for Glaucoma Diagnosis. *Am. J. Appl. Sci.* **2014**, *11*, 248–257. [[CrossRef](#)]
47. Mookiah, M.R.; Acharya, U.R.; Lim, C.M.; Petznick, A.; Suri, J.S. Data mining technique for automated diagnosis of glaucoma using higher order spectra and wavelet energy features. *Knowl.-Based Syst.* **2012**, *33*, 73–82. [[CrossRef](#)]
48. Danandeh Mehr, A.; Rikhtehgar Ghiasi, A.; Yaseen, Z.M.; Sorman, A.U.; Abualigah, L. A novel intelligent deep learning predictive model for meteorological drought forecasting. *J. Ambient. Intell. Humaniz. Comput.* **2022**, *24*, 1–5. [[CrossRef](#)]
49. Gharaibeh, M.; Almahmoud, M.; Ali, M.Z.; Al-Badarneh, A.; El-Heis, M.; Abualigah, L.; Altalhi, M.; Alaiad, A.; Gandomi, A.H. Early Diagnosis of Alzheimer's Disease Using Cerebral Catheter Angiogram Neuroimaging: A Novel Model Based on Deep Learning Approaches. *Big Data Cogn. Comput.* **2021**, *6*, 2. [[CrossRef](#)]
50. Gandomi, A.H.; Chen, F.; Abualigah, L. Machine Learning Technologies for Big Data Analytics. *Electronics* **2022**, *11*, 421. [[CrossRef](#)]
51. Houssein, E.H.; Hassaballah, M.; Ibrahim, I.E.; Abdelminaam, D.S.; Wazery, Y.M. An automatic arrhythmia classification model based on improved Marine Predators Algorithm and Convolutions Neural Networks. *Expert Syst. Appl.* **2022**, *187*, 115936. [[CrossRef](#)]
52. Houssein, E.H.; Abdelminaam, D.S.; Hassan, H.N.; Al-Sayed, M.M.; Nabil, E. A Hybrid Barnacles Mating Optimizer Algorithm with Support Vector Machines for Gene Selection of Microarray Cancer Classification. *IEEE Access* **2021**, *9*, 64895–64905. [[CrossRef](#)]
53. Houssein, E.H.; Abdelminaam, D.S.; Ibrahim, I.E.; Hassaballah, M.; Wazery, Y.M. A Hybrid Heartbeats Classification Approach Based on Marine Predators Algorithm and Convolution Neural Networks. *IEEE Access* **2021**, *9*, 86194–86206. [[CrossRef](#)]
54. Elminaam, D.A.; Ibrahim, S.A. Building a robust heart diseases diagnose intelligent model based on RST using lem2 and modlem2. In Proceedings of the 32nd IBIMA Conference, Seville, Spain, 15–16 November 2018; pp. 5733–5744.
55. Abd Elminaam, D.S.; Elashmawi, W.H.; Ibraheem, S.A. HMFC: Hybrid MODLEM-Fuzzy Classifier for Liver Diseases Diagnose. *Int. Arab. J. E Technol.* **2019**, *5*, 100–109.
56. Nadimi-Shahraki, M.H.; Taghian, S.; Mirjalili, S.; Ewees, A.A.; Abualigah, L.; Elaziz, M.A. MTV-MFO: Multi-Trial Vector-Based Moth-Flame Optimization Algorithm. *Symmetry* **2021**, *13*, 2388. [[CrossRef](#)]
57. Nadimi-Shahraki, M.H.; Taghian, S.; Mirjalili, S.; Abualigah, L.; Elaziz, M.A.; Oliva, D. EWOA-OPF: Effective Whale Optimization Algorithm to Solve Optimal Power Flow Problem. *Electronics* **2021**, *10*, 2975. [[CrossRef](#)]
58. Nadimi-Shahraki, M.H.; Fatahi, A.; Zamani, H.; Mirjalili, S.; Abualigah, L. An Improved Moth-Flame Optimization Algorithm with Adaptation Mechanism to Solve Numerical and Mechanical Engineering Problems. *Entropy* **2021**, *23*, 1637. [[CrossRef](#)] [[PubMed](#)]
59. Elminaam, D.S.A.; Neggaz, N.; Ahmed, I.A.; Abouelyazed, A.E.S. Swarming Behavior of Harris Hawks Optimizer for Arabic Opinion Mining. *Comput. Mater. Contin.* **2021**, *69*, 4129–4149. [[CrossRef](#)]

60. Abdelminaam, D.S.; Neggaz, N.; Gomaa, I.A.E.; Ismail, F.H.; Elsayy, A. AOM-MPA: Arabic Opinion Mining using Marine Predators Algorithm based Feature Selection. In Proceedings of the 2021 International Mobile, Intelligent, and Ubiquitous Computing Conference (MIUCC), Cairo, Egypt, 26–27 May 2021; pp. 395–402. [[CrossRef](#)]
61. Shaban, H.; Houssein, E.H.; Pérez-Cisneros, M.; Oliva, D.; Hassan, A.Y.; Ismaeel, A.A.K.; Abdelminaam, D.S.; Deb, S.; Said, M. Identification of Parameters in Photovoltaic Models through a Runge Kutta Optimizer. *Mathematics* **2021**, *9*, 2313. [[CrossRef](#)]
62. Deb, S.; Houssein, E.H.; Said, M.; Abdelminaam, D.S. Performance of Turbulent Flow of Water Optimization on Economic Load Dispatch Problem. *IEEE Access* **2021**, *9*, 77882–77893. [[CrossRef](#)]
63. Abdul-Minaam, D.S.; Al-Mutairi, W.M.E.S.; Awad, M.A.; El-Ashmawi, W.H. An Adaptive Fitness-Dependent Optimizer for the One-Dimensional Bin Packing Problem. *IEEE Access* **2020**, *8*, 97959–97974. [[CrossRef](#)]
64. El-Ashmawi, W.H.; Elminaam, D.S.A.; Nabil, A.M.; Eldesouky, E. A chaotic owl search algorithm based bilateral negotiation model. *Ain Shams Eng. J.* **2020**, *11*, 1163–1178. [[CrossRef](#)]
65. Acharya, U.R.; Dua, S.; Du, X.; Chua, C.K. Automated diagnosis of glaucoma using texture and higher order spectra features. *IEEE Trans. Inf. Technol. Biomed.* **2011**, *15*, 449–455. [[CrossRef](#)]
66. Acharya, U.R.; Ng, E.Y.; Eugene, L.W.; Noronha, K.P.; Min, L.C.; Nayak, K.P.; Bhandary, S.V. Decision support system for the glaucoma using Gabor transformation. *Biomed. Signal Process. Control* **2015**, *15*, 18–26. [[CrossRef](#)]
67. Yadav, D.; Sarathi, M.P.; Dutta, M.K. Classification of glaucoma based on texture features using neural networks. In Proceedings of the 2014 Seventh International Conference on Contemporary Computing (IC3), Noida, India, 7–9 August 2014; pp. 109–112.
68. Maheshwari, S.; Pachori, R.B.; Kanhangad, V.; Bhandary, S.V.; Acharya, U.R. Iterative variational mode decomposition based automated detection of glaucoma using fundus images. *Comput. Biol. Med.* **2017**, *88*, 142–149. [[CrossRef](#)]
69. Bajwa, M.N.; Malik, M.I.; Siddiqui, S.A.; Dengel, A.; Shafait, F.; Neumeier, W.; Ahmed, S. Two-stage framework for optic disc localization and glaucoma classification in retinal fundus images using deep learning. *BMC Med. Inform. Decis. Mak.* **2019**, *19*, 1–6.
70. Shehab, M.; Abualigah, L.; Shambour, Q.; Abu-Hashem, M.A.; Shambour, M.K.Y.; Alsalibi, A.I.; Gandomi, A.H. Machine learning in medical applications: A review of state-of-the-art methods. *Comput. Biol. Med.* **2022**, *145*, 105458. [[CrossRef](#)] [[PubMed](#)]
71. Ezugwu, A.E.; Ikotun, A.M.; Oyelade, O.O.; Abualigah, L.; Agushaka, J.O.; Eke, C.I.; Akinyelu, A.A. A comprehensive survey of clustering algorithms: State-of-the-art machine learning applications, taxonomy, challenges, and future research prospects. *Eng. Appl. Artif. Intell.* **2022**, *110*, 104743. [[CrossRef](#)]
72. Liu, Q.; Li, N.; Jia, H.; Qi, Q.; Abualigah, L. Modified Remora Optimization Algorithm for Global Optimization and Multilevel Thresholding Image Segmentation. *Mathematics* **2022**, *10*, 1014. [[CrossRef](#)]
73. Gharaibeh, M.; Alzu'Bi, D.; Abdullah, M.; Hmeidi, I.; Al Nasar, M.R.; Abualigah, L.; Gandomi, A.H. Radiology Imaging Scans for Early Diagnosis of Kidney Tumors: A Review of Data Analytics-Based Machine Learning and Deep Learning Approaches. *Big Data Cogn. Comput.* **2022**, *6*, 29. [[CrossRef](#)]
74. Zhang, W.; Li, X.; Ma, H.; Luo, Z.; Li, X. Universal Domain Adaptation in Fault Diagnostics with Hybrid Weighted Deep Adversarial Learning. *IEEE Trans. Ind. Inform.* **2021**, *17*, 7957–7967. [[CrossRef](#)]
75. Zhang, W.; Li, X.; Li, X. Deep learning-based prognostic approach for lithium-ion batteries with adaptive time-series prediction and online validation. *Measurement* **2020**, *164*, 108052. [[CrossRef](#)]